Steel and Composite Structures, *Vol. 26, No. 3 (2018) 329-345*
DOI: https://doi.org/10.12989/scs.2018.26.3.329

Cyclic response and design procedure of a weak-axis cover-plate moment connection

Linfeng Lu [*1], Yinglu Xu [1a], Huixiao Zheng [1b] and James B.P. Lim [2c]

[1] *School of civil engineering, Chang'an University, 75 Chang'an Middle Rd, Xi'an, P.R. China*
[2] *Department of Civil and Environmental Engineering, University of Auckland (City Campus), Engineering Building, 20 Symonds Street, Auckland, New Zealand*

(*Received July 29, 2017, Revised October 11, 2017, Accepted November 7, 2017*)

Abstract. This paper systematically investigated the mechanical performance of the weak-axis cover-plate connection, including a beam end monotonic loading test and a column top cyclic loading test, and a series of parametric studies for exterior and interior joints under cyclic loading using a nonlinear finite element analysis program ABAQUS, focusing on the influences of the shape of top cover-plate, the length and thickness of the cover-plate, the thickness of the skin plate, and the steel material grade. Results showed that the strains at both edges of the beam flange were greater than the middle's, thus it is necessary to take some technical methods to ensure the construction quality of the beam flange groove weld. The plastic rotation of the exterior joint can satisfy the requirement of FEMA-267 (1995) of 0.03 rad, while only one side connection of interior joint satisfied ANSI/AISC 341-10 under the column top cyclic loading. Changing the shape or the thickness or the length of the cover-plate did not significantly affect the mechanical behaviors of frame joints no matter in exterior joints or interior joints. The length and thickness of the cover-plate recommended by FEMA 267 (1995) is also suitable to the weak-axis cover-plate joint. The minimum skin plate thickness and a design procedure for the weak-axis cover-plate connections were proposed finally.

Keywords: steel frame; weak-axis connection; bending connection; panel zone; I-section column; H-shaped beam

1. Introduction

After observing the relatively poor performance of "pre-Northridge" moment connections during 1994 Northridge earthquake, various types of connections based on two concepts of (i) strengthening the connection; and (ii) weakening the beam ends were proposed. For instances, external stiffener connection (Rezaifar and Younesi 2016), T-RBS connection (Ataollahi and Banan 2016), Tubular Web RBS connection (Zahrai *et al*. 2017a, b), and cap plate and extended end plate connections (Nassani *et al*. 2017). But the most of the connections mentioned above basically stay in researching status and are not widely accepted in design specification and practical projects.

The most common failure mode was brittle fracture initiating near the edge of the beam flange groove weld. The cause was large stress concentrations due to force flow towards the stiffer column flanges, which is the opposite pattern as strong-axis moment connections. Driscoll and Beedle (1982) reported that the triaxial tension stresses distribution along the diaphragm displayed as Fig. 1(b) for weak-axis connections and reached a maximum at the edge of the beam flange groove weld (see Fig. 1(b)). While for strong-axis moment connections, this phenomenon reversed with the highest stresses flowing towards the center of the groove weld (see Fig. 1(a)). Since the start and finish are the most critical parts of a weld, the strain concentration pattern of weak-axis moment connections makes them highly susceptible to brittle fracture of the beam flange groove weld. That opinion was proved again in FEMA-355D (2000).

One of the new connection forms, entitled the cover-plate connection, which is getting popular after the Northridge earthquake and is commonly used in present steel frames in China, involves two cover-plates on the beam flanges ends. In this way, the plastic hinge is forced to move away from the column-to-beam flange groove welds, allowing stable yielding of the beam. The cover-plate design has demonstrated successful behavior in laboratory tests involving strong-axis moment connections (Engelhardt and Sabol 1998, Kim *et al*. 2002). When the H-shaped beam with cover-plate is framed into the weak-axis of the I-section column, however, rare information on weak-axis cover-plate connection has been reported except some research paper belongs to the author's research team.

Lu *et al*. (2016, 2017) reported a series of tests on weak axis moment connections, which involved a weak-axis cover-plate connection (see Fig. 2), and confirmed that it had the good plastic rotational capability. Xu *et al*. (2016) have studied the influencing factors on the hysteretic behavior of weak-axis cover-plate connections of the exterior joint in frame, but further studies for the interior joint and also the comparative analysis for exterior and

*Corresponding author, Ph.D., Professor,
E-mail: lulinfeng@chd.edu.cn
[a] Ph.D. Student, E-mail: 2015028003@chd.edu.cn
[b] Ph.D., Associate Professor,
E-mail: james.lim@auckland.ac.nz

ISSN: 1229-9367 (Print), 1598-6233 (Online)

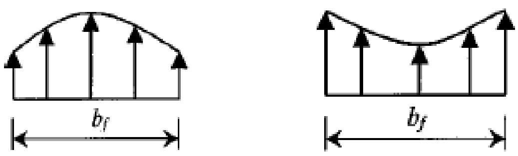

(a) (b)

Fig. 1 Stress profile across beam flange

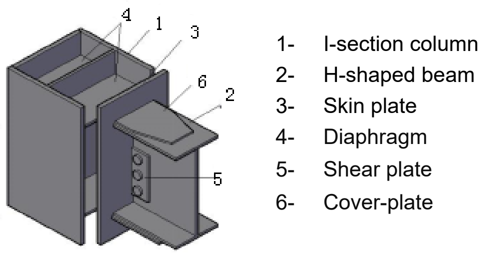

Fig. 2 Weak-axis cover-plate connection

Fig. 3 Test setup of beam end monotonic loading

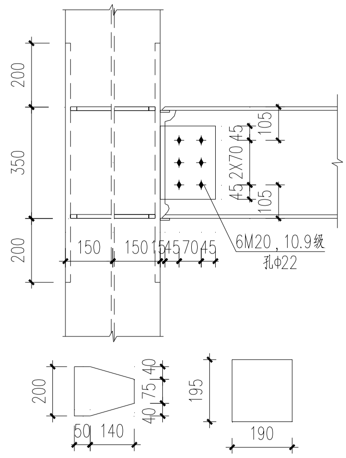

Fig. 4 Details of specimen SJ-2

interior joints are still essential.

Based on the experimental researches done by Lu *et al.* (2016, 2017), this paper will introduce some key technical test data that had never been reported, and conduct a parametric analysis using numerical methods for the proposed weak-axis cover-plate connection to sum critical factors and develop the design procedure for this connection. In this paper, it is necessary to point out that the geometric unit is millimeter if a geometric dimension has no unit mark, and some notation calculation method, such as joint rotation angle (θ), joint plastic rotation angle (θ_p), ductility coefficient (ultimate displacement divided by yield displacement) and other notations shown in the following figures and tables, have been reported in the references (Lu *et al*. 2016, 2017 and Xu *et al*. 2016).

2. Experimental and numerical analysis on the frame exterior joints

A sires of full scale specimens used weak-axis cover-plate connection (see Fig. 2), including a beam end monotonic loading test specimen and some cyclic loading numerical analysis specimens, which were designed and constructed under the assumption that the moment inflection points are close to the mid-height and mid-span of columns and beams respectively in a frame.

2.1 Experimental analysis on a frame exterior joint under beam end monotonic loading

In order to investigate the basic mechanical behavior of the proposed weak-axis cover-plate connection details, specimen SJ-2, shown in Fig. 3, a frame exterior frame joint had been tested under beam end monotonic loading (see Fig. 3). The load was applied vertically at the beam end, with the top and bottom of the column being pin connections, and a vertical hydraulic jack was used to apply an axial force with a compression ratio of 0.3 on the top of the column to simulate the effect of the upper floors in a multi-story building. I-section Q235 steel column with section of HW300×300×10×15 (height: 3000 mm, calculated from the upper hinge point to the lower hinge point) and H-shaped Q235 steel beams with section of HN 350×175×7×11 (span: 1500 mm) were used; the steel plates, too, were made of Q235 steel with nominal yield strength of 235 MPa. In detail, the shear plate and the diaphragms of the column were 12 mm thickness, and the skin plates were 16 mm thickness, and the cover-plates were 6 mm thickness. Fig. 4 gives the geometrical details of specimen SJ-2 with the cover-plate connection.

The failure mode of specimen SJ-2 is shown in Fig. 5(a). It can be observed that the extensive local buckling occurred in the lower beam flange, indicating that under beam end monotonic loading, the proposed connection could induce the plastic hinge at the beam section away from the face of the column.

One of the research aims was to investigate the stress distribution of groove weld, seven strain gauges were located at the beam-to-column connection since they were close and the strain profile across beam flange is shown in Fig. 6. It can be seen that the strain profile and size of the top and bottom beam flange are basically alike expect for

(a) Test

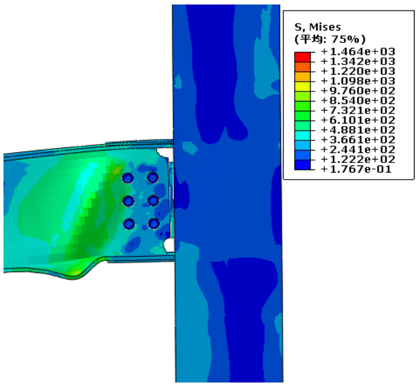

(b) Numerical analysis

Fig. 5 Failure modes of specimen SJ-2 under beam end monotonic loading

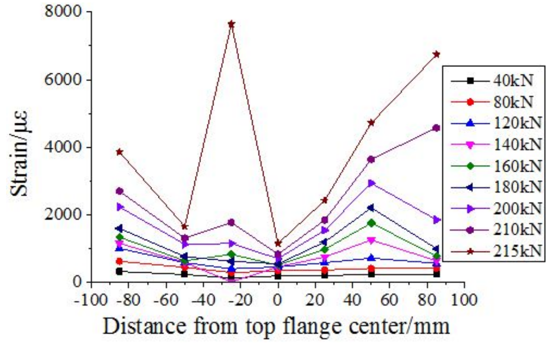

(a) Top beam flange

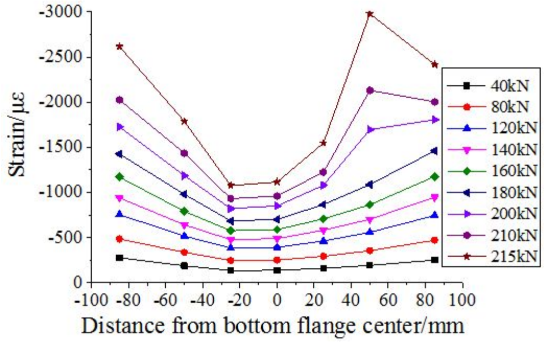

(b) Bottom beam flange

Fig. 6 Strain profile of beam flanges in specimen SJ-2

some individual points and the elastic strain profiles were more regular in the initial loading period. In the elastic-plastic stage, the strains at both edges of the beam flange are greater than the middle's. Some bad strain gauges lead to individual data being anomaly larger, but it still can be seen that they reached the maximum value at the edge of the beam flange groove weld like Fig. 1(b). Therefore, it is necessary to take some technical methods to ensure the construction quality of the beam flange groove weld, such as using a backing plate and removing it after weld metal deposition become cool. If the backing plate is retained, the weld construction shortcoming always exists and the weld crack will occur and transfer from backing plate to groove weld.

2.2 Numerical analysis on frame exterior joints under beam end loading

In order to study the cyclic response of frame exterior joints with weak-axis cover-plate connection, an analytical study using a refined tridimensional model was conducted using a general-purpose nonlinear finite element analysis program ABAQUS. Eight-node solid nonconforming elements C3D8I were used to reduce the number of grid units and shorten the calculation time. The plasticity model was based on the Von Mises yielding criteria and the associated flow rule.

2.2.1 Numerical analysis validation under beam end monotonic loading

The average material properties from steel coupon test of specimen SJ-2 and high-strength bolt mechanical property had been given by Lu *et al.* (2016). The failure mode in numerical analysis is displayed in Fig. 5(b). Comparing the deformation configuration of the test and numerical analysis in Fig. 5, the predicted failure mode of numerical analysis demonstrated a good correlation with the test. Under the beam end monotonic loading, beam bottom flange and web experienced substantial local buckling deformations with the panel zone mainly being in the elastic state. Global behavior of the connection in test and FEM was presented in terms of load-displacement hysteretic loops at the loading point, as shown in Fig. 7. It can be observed that the numerical results have good agreement with the test results, especially in the elastic stage that the numerical model could accurately simulate the initial stiffness of the load-displacement hysteresis curves, indicating that the Young's modulus and the Poisson's ratio

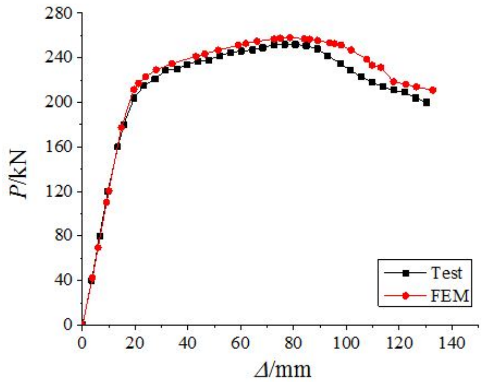

Fig. 7 Beam end load versus displacement relationships of test and FEM analysis

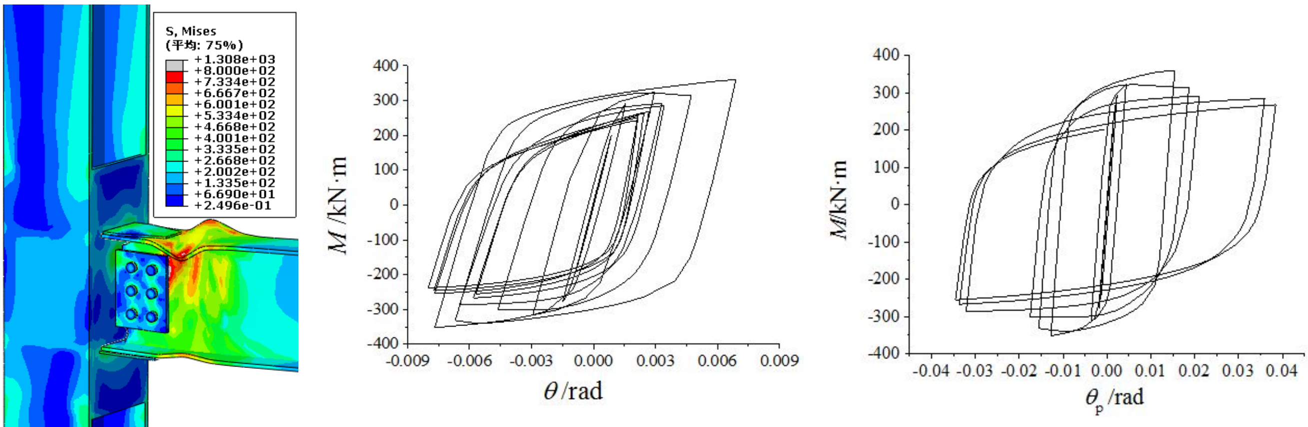

(a) Failure mode (b) M-θ curve (c) M-θ_p curve

Fig. 8 Cyclic responses of cover-plate connection specimen SJ-2 under beam end cyclic loading

of the material were real and effective. And the inelastic response of the connection in FEM showed the same trend as test results. As expected, the modelling result was slightly higher than that of the test for the plastic part, which was common and principally because simplifications were adopted in FEM to facilitate the creation of the geometry, the definition of material properties and boundary conditions. The maximum error of the load was 2.4%, no more than 5%, demonstrating good correlation between the test and FEM.

2.2.2 Numerical analysis of specimen SJ-2 under beam end cyclic loading

Using the analysis method given by Xu *et al*. (2016), the failure mode of specimen SJ-2 under beam end cyclic loading is displayed in Fig. 8(a). The curve of moment-rotation angle (M-θ) and the curve of moment-plastic rotation angle (M-θ_p) under cyclic loading are also shown in Figs. 8(b) and (c). Since the sizes of the top and bottom cover-plate are different, they lead to the different position of the plastic hinge at the top beam flange and bottom beam flange respectively, so that the rotation angles are different in the two loading directions, as shown in Fig. 8(b). In the early stage of loading, the M-θ curve is basically symmetrical, but upon further loading, the hysteresis curve is no longer symmetrical, which reflected the cover-plate size influence on the rotational stiffness of joint. It can be calculated form Fig. 8(c) that the maximum positive plastic rotation was 0.038 rad and the minimum negative plastic rotation was -0.035 rad, which means the plastic rotation of the joint can satisfy the requirement of FEMA-267 (1995).

3. Experimental and numerical analysis on frame interior joints under column top cyclic loading

3.1 Experimental analysis on a frame interior joint under column top cyclic loading

The majority of previous tests reported were about exterior frame joints with less attention being paid to interior frame joints, the most commonly used in actual engineering steel frames. In order to study the cyclic response of frame interior joints with weak-axis cover-plate connection under earthquake effect, the test setup was designed to reproduce the boundary conditions of a beam-to-column connection substructure in a moment-resisting frame under earthquake loading, thus, the beam was assumed to be pin-supported at mid-span points, and the tip of the column was loaded horizontally at an assumed pin at its mid-height, and also the bottom of the column was hinged, as shown in Fig. 9. A hydraulic actuator was arranged for horizontal cyclic loading placed at the top of the column to consider the P–delta effect so as to better simulate the real situation of structural loading as columns drift laterally under seismic loads in real steel frames. The specimen was assembled from two 1500 mm long HN 350×175×7×11 beams and one 4030 mm height HW 350×350×12×19 column to form the cruciform arrangement, and all steel members were fabricated using Q235 with a nominal yield strength of 235 MPa. The beams are connected to the skin plates using the welded-flange bolted-web connection, similar to the specimen of mono-

Fig. 9 Test setup of cyclic loading

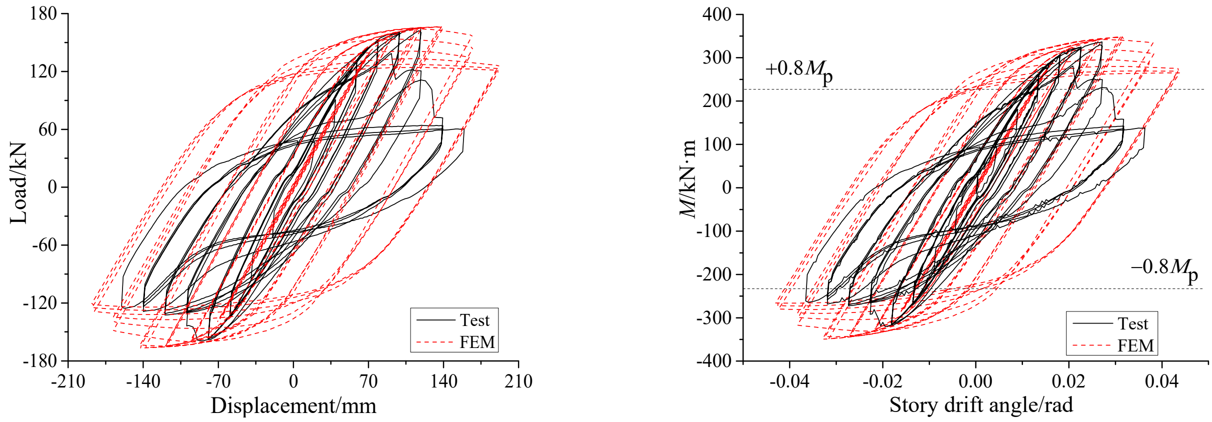

(a) Load-displacement relationships (b) Moment-story drift angle relationships

Fig. 10 Hysteretic loops of the proposed connection under cyclic loading

(a) Weld cracking of diaphragm (b) Weld cracking and skin plate tearing (c) Ultimate failure mode

Fig. 11 Failure patterns of specimen SJ-3

tonic loading test. For brevity, only the most significant results never reported of the cover-plate interior joint specimen SJ-3 are commented upon. Much additional information could be found in the companion paper by Lu *et al*. (2017).

3.1.1 Test results

The hysteretic loops of the column top load versus the controlled horizontal displacement and moment versus story drift angle are plotted in Fig. 10. It can be seen form Fig. 10(a) that the load-displacement hysteresis loops were stable and repetitive before the horizontal displacement reaching 100 mm, and minor local buckling of beam bottom flange could be noticed in the cycles of 100 mm. Then the weld between the diaphragm and the skin plate cracked (see Fig. 11(a)) with a metallic grating noise, leading to a drastic drop of bearing capacity (see Figs. 10(a) and (b)). And a crack developed in the left beam bottom flange weld during the following loading cycles, resulting in the tearing of the skin plate (see Fig. 11(b)). In ANSI/AISC 341-10 (2010), the beam-to-column connections for special moment frames shall be capable of accommodating a story drift angle of at least 0.04 rad while the measured flexural resistance of the connection at the face of the column should equal at least 0.80 M_p of the beam. As seen from Fig. 10(b), only the negative bending capacity met that requirement, indicating that the proposed connection could meet the requirement only under good workmanship and welding quality.

Comparing the test results of beam end monotonic loading and column top cyclic loading, it can be concluded that there was a large discrepancy between them. Under beam end monotonic loading, the panel zone and welds kept in good condition, and beam flanges and web experienced substantial local buckling deformations outside the cover-plate region. While under the column top cyclic loading, the welds between the skin plate and diaphragm cracked and also the beam flange groove welds, and then the tearing occurred in the skin plate, indicating that the beam-column interior joint under the column top cyclic loading was in more serious situation than the beam-column exterior joint under the beam end monotonic loading. However, interior frame joints are commonly used in actual engineering steel frames, thus it is necessary to conduct more research for interior frame joints to ensure the safety of steel frames. Notably, under the column top horizontal cyclic loading, the premature fracture of weld between diaphragm and skin plate caused the early crack in beam flange groove weld, and prevented the development of beam plastic hinge, thus, good workmanship and welding quality is first required to provide a reliable welded connection.

3.1.2 Stress profiles

3.1.2.1 Stress profiles in the panel zone

The panel zone was instrumented extensively with triaxial strain gauges in order to ascertain the strain profiles in the proposed weak-axis cover-plate connection details.

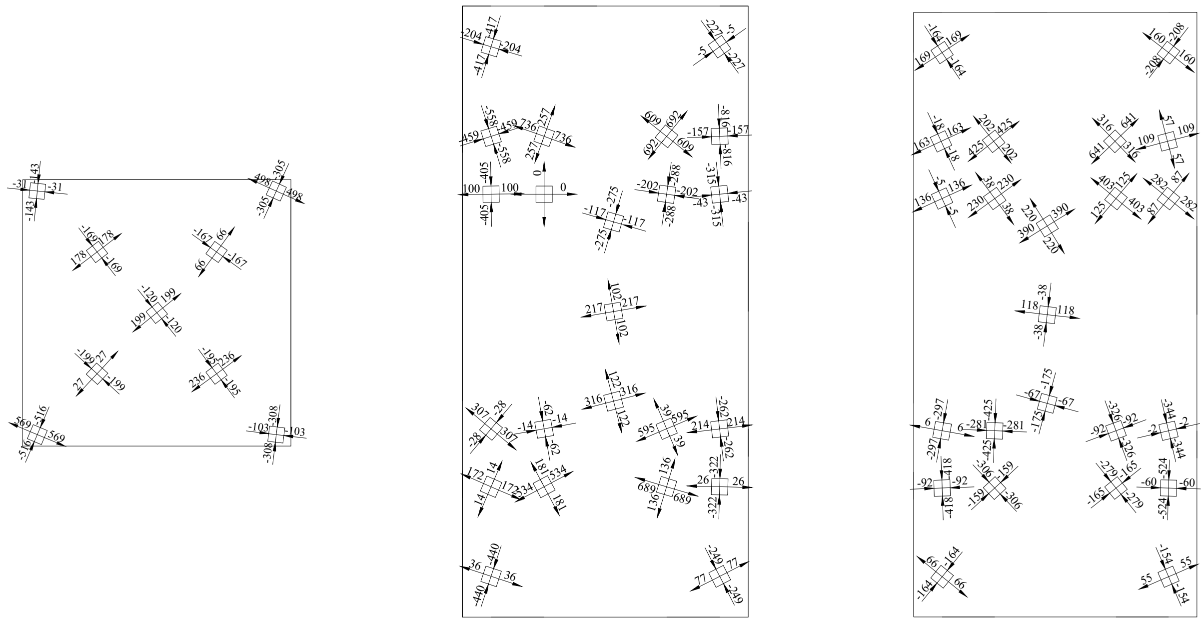

(a) Panel zone (b) Left skin plate (c) Right skin plate

Fig. 12* Stress distribution of panel zone and skin plates of specimen SJ-3

*The arrow is the direction of the principal stress and the number is the stress value in MPa

Based on the measurement of strain gauge rosettes under the maximum load and the obtained steel material properties, the values and directions of stress in the panel zone for the specimen SJ-3 are depicted in Fig. 12(a), where the arrow is the direction of the principal stress and the number is the stress value in MPa. It is observed from Fig. 12(a) that the stresses of other zones were significantly smaller than the steel material yield strength except for higher stress values in four corner zones, illustrating that only tiny elastic shear deformation occurs in the panel zone. Therefore, it can be concluded that the proposed weak-axis cover-plate connection is a kind of strong panel zone connection. Relatively, larger stresses appeared on the four corners of panel zone, which can be attributed to the fact that larger tensile stress and compressive stress in the beam flange groove welds has significant impact on the local stress distribution of the panel zone.

3.1.2.2 Stress profiles in the skin plate

The skin plate is one of the most significant elements in the proposed weak-axis cover-plate connection, thus, it is necessary to investigate the stress profiles on the skin plates. Based on the measurement of strain gauge rosettes under the maximum load and the corresponding material properties, the values and directions of stresses in the skin plates for the specimen SJ-3 are presented in Figs. 12(b) and (c), where the arrow is the direction of the principal stress and the number is the stress value in MPa. As can be observed from Figs. 12(b) and (c), the stress values are larger where the skin plate connected to beam flanges and

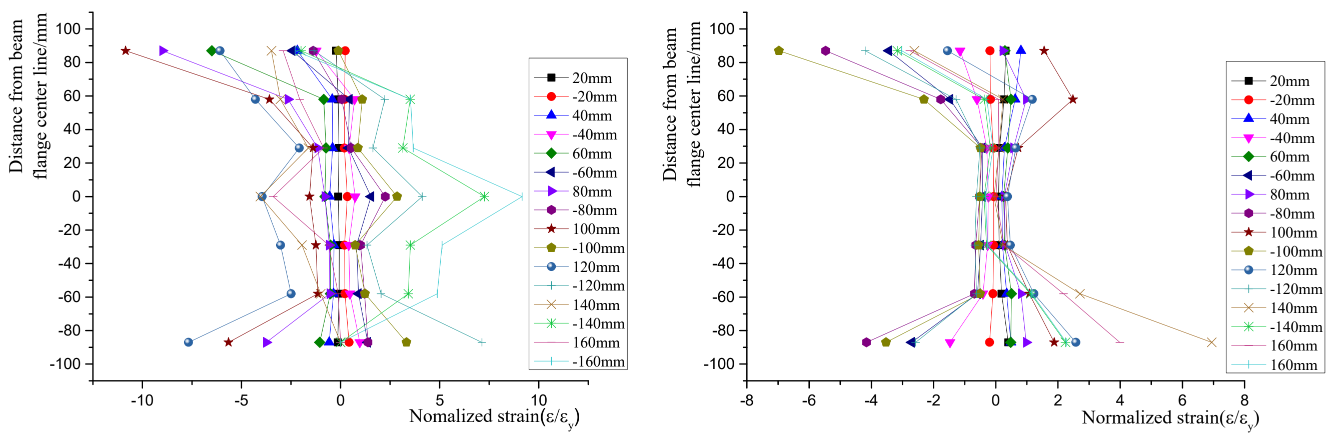

(a) Left beam bottom flange (b) Right beam bottom flange

Fig. 13 Strain profile of beam flanges in specimen SJ-3 the shear plate, and some values are close to or over the steel material yield strength, indicating that the cover-plate was not conducive to reduce the peak stress of the zones where the skin plate was connected with beam flanges, esulting in the tearing in the skin plate in the test. The stresses in the four corners, which are 150 mm away from the top and bottom beam flange, were relatively smaller, indicating that the height of skin plate, which was 200 mm away from the top and bottom beam flange in the tests, can be reduced appropriately.

3.1.3 Strain profiles in the steel beam flange

Seven strain gauges were supposed to be located at the beam-to-column flange groove weld with 29 mm in span, and the strain profiles across the width of beam flange are shown in Fig. 13. In order to show more clearly, the normalized strain (strain ε divided by steel yield strain ε_y) was given at the different loading amplitudes. It can be seen from Fig. 13 that the strains at both edges of the beam flange were greater than the middle's, which was similar to that of monotonic loading. Therefore, it is necessary to take same technical methods suggested in part 2.1 to ensure the construction quality of the beam flange groove weld.

3.1.4 Energy dissipation capacity

Energy dissipation capacity is an important index to evaluate the seismic performance of beam-to-column moment connections, and it can be measured through the area of the load-displacement hysteretic curve. According to JGJ/T 101 (2015), the equivalent viscous damping coefficient (ξ_{eq}) can reflect the energy dissipation capacity. For this interior joint specimen SJ-3, the equivalent viscous damping coefficient under different loading amplitudes is summarized in Table 1.

At the initial stage of loading, the specimen was in the elastic state, the equivalent viscous damping coefficient was at a low level. With the increase of the horizontal loading displacement amplitude, the equivalent viscous damping coefficient gradually increased with the ultimate value greater than 0.2, indicating that the specimen SJ-3 has a good energy dissipation capacity.

Table 1 Equivalent viscous damping coefficient

	Loading step /mm				
ξ_{eq}	20	40	80	120	160
	0.14	0.10	0.13	0.22	0.26

3.2 Numerical analysis on a frame interior joint under column top cyclic loading

Except for nominal stresses and strains of steel material and weld metal deposition are obtained from the coupon tests corresponding to specimen SJ-3, as depicted by Lu *et al* (2017), the other FEM numerical analysis processes of specimen SJ-3 are the same as that of specimen SJ-2 introduced in part 2.

The hysteresis curve of column top load-displacement relationship of the test is shown in Fig. 10(a) with the curve obtained by FEM superimposed. On the basis of these hysteretic loops, skeleton curves of load–displacement relation for test and FEM can be illustrated in Fig. 14(a). As evidenced from Figs. 10(a) and 14(a), the initial stiffness of FEM and test determined by the inclination of the skeleton curve in the elastic stage matched well, indicating that Young's modulus and the Poisson's ratio of the material were real and effective, thus the elastic response of the connection in the test could be simulated precisely. The inelastic response of the connection in FEM shows the same trend as test results although obvious divergences were observed in the plastic part, and predictions in numerical analysis overestimated the actual strength capacity of composite connection. This is mainly due to the weld fracture in the test, resulting in a drastic drop in the bearing capacity, which was hardly simulated in the FEM, thus the skeleton curve was smoother in the FEM. The behavior was close to that of the test in the negative direction, while the differences were more obvious in the positive direction, because of the fact that the early weld crack occurred between the skin plate and diaphragm, and lead to skin plate being torn during the following loading cycling and a drastic drop in bearing capacity, which could not accurately be simulated in the FEM. In general, reasonable correlation between the test and FEM was observed, and the results of FEM satisfactorily represented the connection behavior. Although the damage of skin plate and welds were not simulated, and the material properties were simplified in the FEM analysis, but the likelihood of fracture could be evaluated through the stress profile, such as in Fig. 14(c), it can be seen that the stress values in edges of left beam flange groove weld were the highest of all the weld stress profiles.

(a) Skeleton curves (b) Failure mode of test (c) Failure mode of FEM

Fig. 14 Comparison of the skeleton curves and failure modes

Table 2 Details of all series frame joints

Member	Section of column	Section of beam	Skin plate	Diaphragm	Bottom cover-plate	Top cover-plate
ECPS-1	HW300×300×10×15	HN350×175×7×11	-270×750×16	-129×270×12	-190×195×6	Fig. 15(a)
ECPS-2	HW300×300×10×15	HN350×175×7×11	-270×750×16	-129×270×12	-190×195×6	Fig. 15(b)
ECPS-3	HW300×300×10×15	HN350×175×7×11	-270×750×16	-129×270×12	-190×195×6	Fig. 15(c)
ECPL-1	HW300×300×10×15	HN350×175×7×11	-270×750×16	-129×270×12	-160×195×6	-160×155×6
ECPL-2	HW300×300×10×15	HN350×175×7×11	-270×750×16	-129×270×12	-190×195×6	Fig. 15(c)
ECPL-3	HW300×300×10×15	HN350×175×7×11	-270×750×16	-129×270×12	-220×195×6	-220×155×6
ECPT-1	HW300×300×10×15	HN350×175×7×11	-270×750×16	-129×270×12	-190×195×4	-190×155×4
ECPT-2	HW300×300×10×15	HN350×175×7×11	-270×750×16	-129×270×12	-190×195×4	Fig. 15(c)
ECPT-3	HW300×300×10×15	HN350×175×7×11	-270×750×16	-129×270×12	-190×195×4	-190×155×8
ECPT-4	HW300×300×10×15	HN350×175×7×11	-270×750×16	-129×270×12	-190×195×4	-190×155×10
EST-1	HW300×300×10×15	HN350×175×7×11	-270×750×10	-129×270×12	-190×195×6	Fig. 15(b)
EST-2	HW300×300×10×15	HN350×175×7×11	-270×750×12	-129×270×12	-190×195×6	Fig. 15(b)
EST-3	HW300×300×10×15	HN350×175×7×11	-270×750×14	-129×270×12	-190×195×6	Fig. 15(b)
EST-4	HW300×300×10×15	HN350×175×7×11	-270×750×16	-129×270×12	-190×195×6	Fig. 15(b)
ESM-1	HW300×300×10×15	HN350×175×7×11	-270×750×12	-129×270×12	-190×195×6	Fig. 15(b)
ESM-2	HW300×300×10×15	HN350×175×7×11	-270×750×14	-129×270×12	-190×195×6	Fig. 15(b)
ESM-3	HW300×300×10×15	HN350×175×7×11	-270×750×16	-129×270×12	-190×195×6	Fig. 15(b)
ICPS-1	HW350×350×12×19	HN350×175×7×11	-312×750×16	-153×312×12	-190×195×6	Fig. 15(a)
ICPS-2	HW350×350×12×19	HN350×175×7×11	-312×750×16	-153×312×12	-190×195×6	Fig. 15(b)
ICPS-3	HW350×350×12×19	HN350×175×7×11	-312×750×16	-153×312×12	-190×195×6	Fig. 15(c)
ICPL-1	HW350×350×12×19	HN350×175×7×11	-312×750×16	-153×312×12	-160×155×6	-160×155×6
ICPL-2	HW350×350×12×19	HN350×175×7×11	-312×750×16	-153×312×12	-190×155×6	Fig. 15(c)
ICPL-3	HW350×350×12×19	HN350×175×7×11	-312×750×16	-153×312×12	-220×155×6	-220×155×6
ICPL-4	HW350×350×12×19	HN350×175×7×11	-312×750×16	-153×312×12	-250×155×6	-250×155×6
ICPT-1	HW350×350×12×19	HN350×175×7×11	-312×750×16	-153×312×12	-190×155×6	Fig. 15(c)
ICPT-2	HW350×350×12×19	HN350×175×7×11	-312×750×16	-153×312×12	-190×155×8	-190×155×8
ICPT-3	HW350×350×12×19	HN350×175×7×11	-312×750×16	-153×312×12	-190×155×10	-190×155×10
IST-1	HW350×350×12×19	HN350×175×7×11	-312×750×12	-153×312×12	-190×155×6	Fig. 15(b)
IST-2	HW350×350×12×19	HN350×175×7×11	-312×750×14	-153×312×12	-190×155×6	Fig. 15(b)
IST-3	HW350×350×12×19	HN350×175×7×11	-312×750×16	-153×312×12	-190×155×6	Fig. 15(b)
IST-4	HW350×350×12×19	HN350×175×7×11	-312×750×18	-153×312×12	-190×155×6	Fig. 15(b)

4. Specific parameter numerical analysis on frame joints under cyclic loading

For the weak-axis cover-plate connection proposed in this paper, the cover-plate is the key component in this connection, and the geometrical sizes of the cover-plate may influence the cyclic responses of a frame joint. To better understand the structural behavior of the weak-axis cover-plate connection, it is important to investigate the joints with systematic parametric studies. Table 2 shows the different parameters selected for numerical analysis. In Table 2, the specimen number was designated as: in “ECP” or “ICP” series joints, “E” represents the exterior joint, “I” represents the interior joint, “L” represent the length of the cover plate, “CP” represents the cover-plate, “S” represents the shape of the top cover-plate, and “T” represents the thickness of the cover-plate; in “ES” or “ IS” series joints, “S” represents the skin plate, “T” represents the thickness of the skin plate, “M” represents the steel material grade. They are considered to be the most influential factors for the weak-axis cover-plate connection. Only one variable was changed at one series joints so as to assess its effect clearly.

The material properties of the exterior frame joint specimen SJ-2 and the interior frame joint specimen SJ-3 have been given in Lu *et al*. (2016) and Lu *et al*. (2017) respectively. The procedures for calculating the yield displacement were similar to those described by Shim (2014), but the ultimate displacement was defined as the displacement with 15% decrease in loading after the maximum loading. A systemic parametric study was carried out to investigate the structural behavior with variations in: shape of the top cover-plate, length of the cover-plate, thickness of the cover-plate and the skin plate, and also the steel material grade. Analysis results were descripted for exterior joints and interior joints in pairs to compare the influence difference of various parameters. Notably, for in

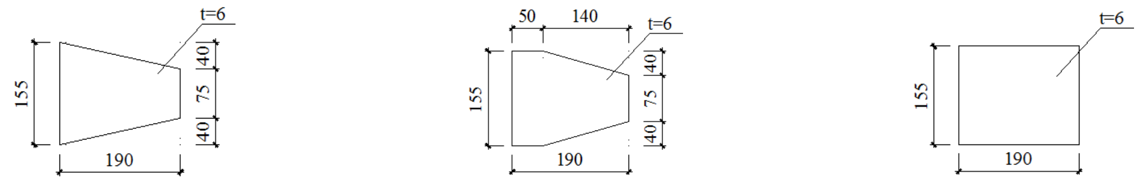

(a) Trapezoid cover-plate (b) Wedge cover-plate (c) Rectangle cover-plate

Fig. 15 Shapes and sizes of top cover-plate

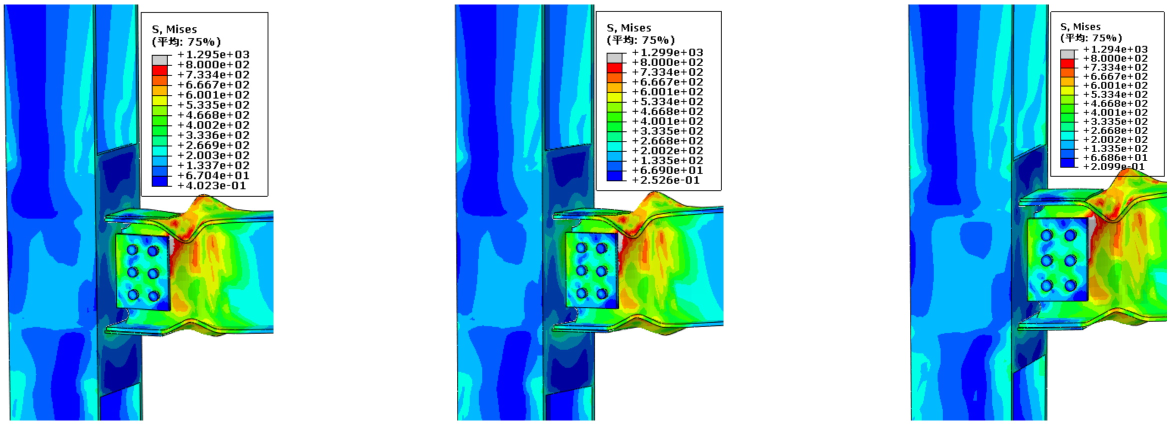

(a) ECPS-1 (b) ECPS-2 (c) ECPS-3

Fig. 16 Failure modes of ECPS series joints

agreement with the experimental tests, exterior joints were applied beam end cyclic loading and interior joints applied column top cyclic loading in FEM.

4.1 The influences of top cover-plate shape

For welding convenience, the top cover-plate is always narrower than the top beam flange, and the bottom cover-plate is often wider than the bottom beam flange. There are three types of the top cover-plate, including the trapezoid plate, wedge plate, and rectangle plate, while the bottom cover-plate is often a rectangular plate. In order to investigate the influences of top cover-plate shape on the cyclic response of weak-axis cover-plate connection, three exterior frame joints (ECPS series) and three interior frame joints (ICPS series) have been analyzed, as listed in Table 2, and geometrical dimensions of the three types of top cover-plates are shown in Fig. 15.

4.1.1 The influences on exterior frame joints

Failure modes of ECPS series joints are shown in Fig. 16, and the analysis results of exterior frame joints were summarized in Table 3. It can be observed from Fig. 16 and Table 3 that changing of the top cover-plate shape slightly affected the initial rotation stiffness, bearing capacity and ductility, moreover, the maximum plastic rotation angles of the three joints were all greater than 0.03 rad, which satisfies the requirement of FEMA267 (1995).

4.1.2 The influences on interior frame joints

The failure modes of ECPS series joints are shown in Fig. 17, and the analysis results of interior frame joints were summarized in Table 4. The figures and the analysis results declared that the influence of the top cover-plate shape on the cyclic behavior was basically the same as that of exterior frame joints.

To sum up, changing the shape of the top cover-plate did not significantly affect the mechanical behaviors of frame joints no matter in exterior joints or interior joints which use I-section column and weak-axis cover-plate connection. However, trapezoidal and wedge cover-plates can reduce the total length of the fillet welds, and also can reduce the welding heat influence on the beam flange steel, but the rectangular cover-plate is more convenient to manufacture.

4.2 The influences of cover-plate length

For strong-axis cover-plate moment connection of I-section column, FEMA 267 (1995) recommended that the minimum length of cover-plate had better equal to 0.5-time beam height of H-shape beam. The ECPL series joints and the ICPL series joints were designed in order to better understand the mechanical behavior of weak-axis cover-plate connection with different length of the cover-plate. Based on the conclusion in part 4.1, the rectangular cover-plate was adopted in these two series joints due to its convenient, and the details are listed in Table 2.

4.2.1 The influences on exterior frame joints

The failure modes of ECPL series joints are shown in Fig. 18, and the numerical analysis results are listed in Table 3. It can be seen from Fig. 18 that the plastic hinges formed in the beam flanges and web beyond the cover-plate

Table 3 Numerical analysis results of all series exterior frame joints

	Initial rotation stiffness /kN·m.rad^{-1}	Yield moment /kN·m	Yield rotation angle /rad	Ultimate moment /kN·m	Ultimate rotation angle /rad	Maximum plastic angle /rad	Ductility coefficient
ECPS-1	219527	289.4	0.0022	349.8	0.0084	0.0313	3.82
ECPS-2	220063	292.9	0.0022	352.3	0.0083	0.0313	3.72
ECPS-3	223509	293.6	0.0022	354.1	0.0081	0.0310	3.68
ECPL-1	212870	286.1	0.0021	345.3	0.0085	0.0327	4.05
ECPL-2	223509	293.6	0.0022	354.1	0.0081	0.0310	3.68
ECPL-3	229250	294.7	0.0020	361.0	0.0076	0.0278	3.62
ECPT-1	210714	281.5	0.0023	338.7	0.0101	0.0319	4.20
ECPT-2	221053	289.9	0.0021	352.3	0.0079	0.0313	3.76
ECPT-3	227627	298.1	0.0019	354.8	0.0061	0.0305	3.21
ECPT-4	233048	302.7	0.0019	359.7	0.0060	0.0291	3.16
EST-1	201038	285.2	0.0023	345.6	0.0072	0.0281	3.13
EST-2	208380	287.8	0.0022	348.3	0.0072	0.0289	3.27
EST-3	213906	290.9	0.0021	351.4	0.0075	0.0304	3.57
EST-4	220063	292.9	0.0022	352.3	0.0083	0.0313	3.72
ESM-1	206852	395.2	0.0024	501.8	0.0087	0.0274	3.65
ESM-2	214473	400.3	0.0022	502.4	0.0074	0.0289	3.36
ESM-3	223302	402.1	0.0021	502.8	0.0069	0.0304	3.29

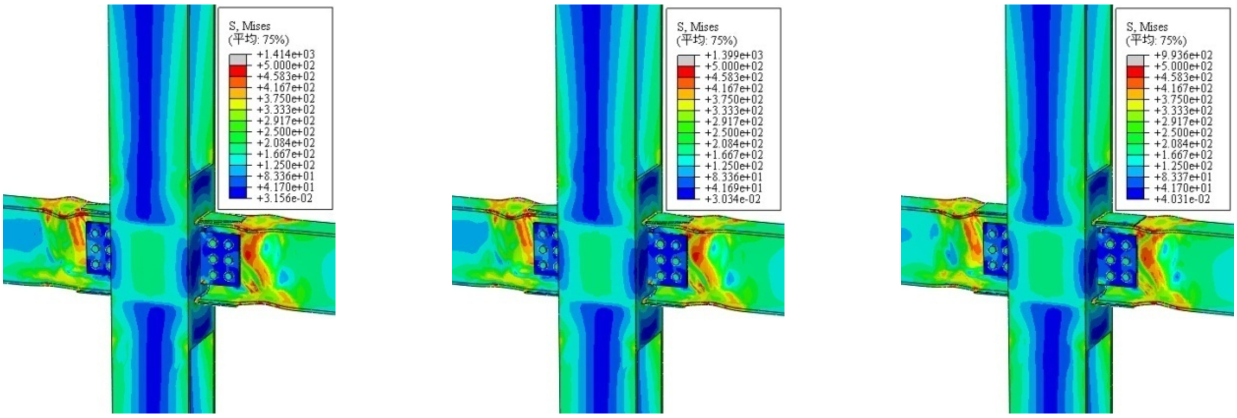

(a) ICPS-1 (b) ICPS-2 (c) ICPS-3

Fig. 17 Failure modes of ICPS series joints

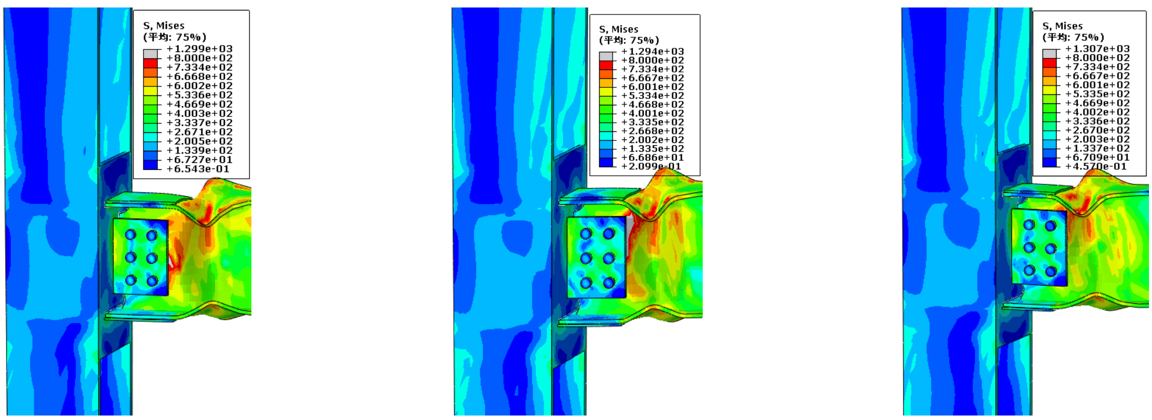

(a) ECPL-1 (b) ECPL-2 (c) ECPL-3

Fig. 18 Failure modes of ECPL series joints

Table 4 The numerical analysis results of all series interior frame joints

	Yield load /kN	Yield displacement /mm	Peak load /kN	Peak displacement /mm	Ultimate load /kN	Ultimate displacement /mm	Ductility coefficient
ICPS-1	134.07	68.55	151.28	119.45	128.59	146.23	2.13
ICPS-2	135.65	68.51	151.31	118.73	128.61	145.29	2.12
ICPS-3	134.64	68.47	151.85	118.67	129.07	144.60	2.11
ICPL-1	132.81	67.48	148.55	119.94	126.26	146.32	2.17
ICPL-2	134.64	68.47	151.85	118.67	129.07	144.60	2.11
ICPL-3	137.53	70.04	155.83	118.58	132.46	146.65	2.09
ICPL-4	140.08	71.22	159.27	118.47	135.38	148.13	2.08
ICPT-1	134.64	68.47	151.85	118.67	129.07	144.60	2.11
ICPT-2	135.36	68.20	152.81	118.11	129.89	138.85	2.04
ICPT-3	137.13	67.93	153.46	118.11	130.44	135.71	2.00
IST-1	-	-	-	-	-	-	-
IST-2	133.23	70.13	150.60	119.74	128.01	151.28	2.16
IST-3	135.65	68.51	151.31	118.73	128.61	145.29	2.12
IST-4	136.60	68.47	151.51	117.27	128.78	144.38	2.10

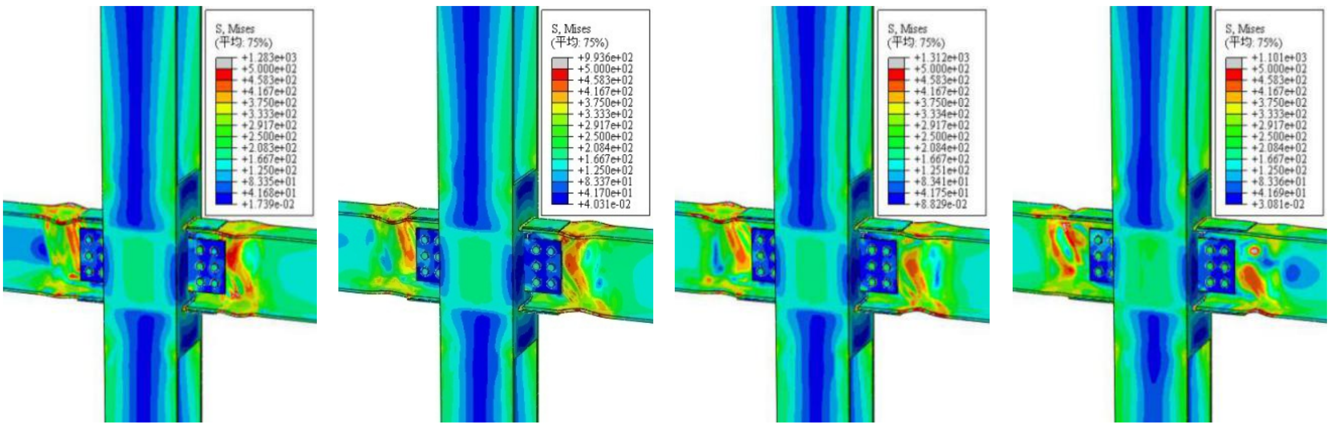

(a) ICPL-1 (b) ICPL-2 (c) ICPL-3 (d) ICPL-4

Fig. 19 Failure modes of ICPL series joints

range with the panel zone being intact in all the ECPL series joints, which can be concluded that changing the length of the cover-plate did not significantly affect the overall failure modes of exterior frame joints. From the calculation data listed in Table 3, changing the length of the cover-plate slightly influenced the stiffness and bearing capacity of the connection, while it had obviously impact on the ductility coefficient and maximum plastic rotation angle. The ductility coefficient of ECPL-1 was 11.8% higher than that of ECPL-3, and the maximum plastic rotation angle of ECPL-1was 17.6% higher than ECPL-3, and the latter did not satisfy the requirement of FEMA 267 (1995). It can be concluded that the length of cover-plate recommended by FEMA267 (1995) is suitable to the weak-axis cover-plate connection.

4.2.2 The influences on interior frame joints

The failure modes of ICPL series joints are shown in Fig. 19, and the analysis results are shown in Table 4. It can be observed that changing the top cover-plate length had similar influence on the cyclic performance of the connection as that of exterior frame joint. Increasing the length of cover-plate slightly decreased the ductility coefficient and plastic rotation capacity of the joint. Fig. 19 also reflects that it is more difficult to form a plastic hinge in the beam flange when the length of cover-plate becomes longer than 0.5-time beam height.

To sum up, increasing the length of cover-plate had a little influence on the bearing capacity of frame joints with weak-axis cover-plate connection. It is suggested that 0.5-time beam height is suitable for the cover-plate length in the proposed weak-axis cover-plate connection.

4.3 The influences of cover-plate thickness

In general, increasing the thickness of the cover-plate would increase the initial rotational stiffness and bearing capacity of the connection, but how it impacts the joint ductility and plastic rotation capacity should be quantified

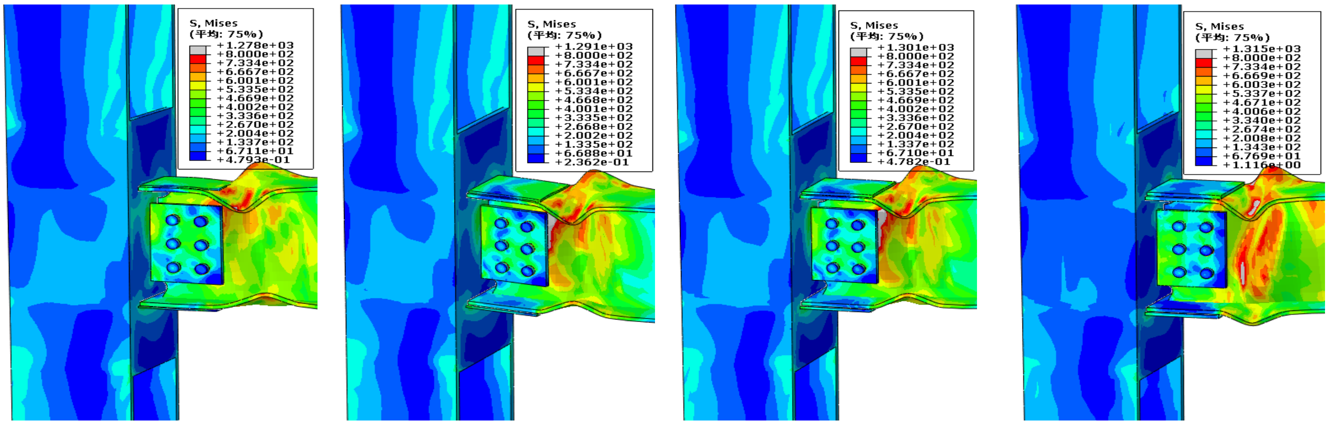

(a) ECPT-1 (b) ECPT-2 (c) ECPT-3 (d) ECPT-4

Fig. 20 Failure modes of ECPT series joints

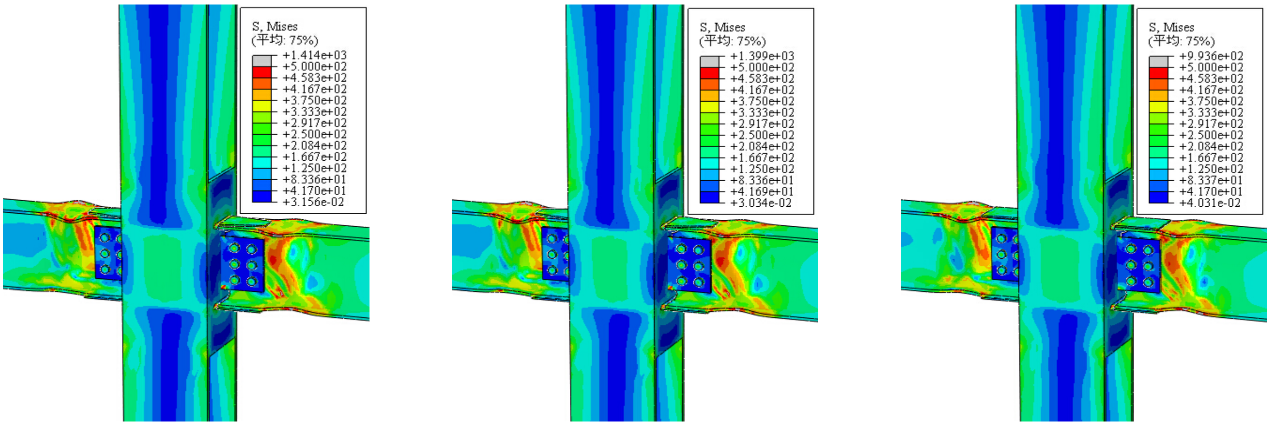

(a) ICPT-1 (b) ICPT-2 (c) ICPT-3

Fig. 21 Failure modes of ICPT series joints

by the numerical analysis. For strong-axis cover-plate connection, FEMA 267 (1995) requires that the sum of the thickness of a cover-plate and a beam flange should not only be greater than twice the thickness of beam flange but also be lower than the thickness of column flange. The ECPT series exterior frame joints only changed the thickness of the top cover-plate, and the ICPT series interior frame joints changed the both thickness of top and bottom cover-plates. Also, the rectangular cover-plates were used in these series joints for convenience. The details of these joints are shown in Table 2.

4.3.1 The influences on exterior frame joints

Failure modes of ECPT series joints are shown in Fig. 20, and the numerical analysis results are listed in Table 3. It can be observed from Fig. 20 that the failure modes of the ECPT series joints and the stress distributions of the skin plates are basically identical, and the plastic hinges formed in the beam flanges and web beyond the cover-plate range. But the stress profiles of cover-plate zone are different, with the increasing of the top cover-plate thickness, the stress in the cover-plate gradually decreased and the stress of the beam flanges and web beyond the cover-plate range increased.

Table 3 indicates that changing the thickness of the top cover-plate obviously affected the initial stiffness and bearing capacity. The initial rotation stiffness of ECPT-4 was10% greater than that of ECPT-1, and ultimate moment of ECPT-4 was 6.2% greater than that of ECPT-1. Furthermore, the ductility coefficient and maximum plastic rotation angle were obviously affected by the top cover-plate thickness change. The ductility coefficient of ECPT-1 was 24.8% higher than that of ECPT-4, with the maximum plastic rotation angle of ECPT-1 9.6% higher than that of ECPT-4, and the latter did not satisfy the requirement of FEMA 267 (1995). It can be concluded that the thickness of the cover-plate recommended by FEMA 267 (1995) is suitable to weak-axis cover-plate exterior frame joints.

4.3.2 The influence on interior frame joints

The failure modes of ICPT series joints are shown in Fig. 21, and the numerical analysis results of ICPT series joints are listed in Table 4. It can be seen form Fig. 21 and Table 4 declared that the influence of the cover-plate thickness on the cyclic behavior of the connection was basically the same as that of exterior frame joint. Increasing the thickness of the cover-plate could significantly enhance the bearing capacity of frame joints. On the other hand, increasing the thickness of the cover-plate could reduce the ductility and plastic rotation capacity of frame joints. Numerical analysis results of ICPT-1 proved that the thickness of cover-plate recommended by FEMA 267 (1995) is suitable to weak-axis cover-plate interior frame joints.

To sum up, the thickness of the cover-plate recommended by FEMA 267 (1995) is also suitable to weak-axis cover-plate frame joints.

5. Calculation formula of skin plate thickness

The out-of-plane stiffness of skin plate is relatively small compared to its plane stiffness, and the out-of-plane stiffness could be decided by the thickness of the skin plate, which will affect the joint rotation stiffness and the plastic hinge occurring in the H-shaped beam. In general, the joint with thick skin plate has a higher bearing capacity, but thin steel plate has well metal quality and mechanical properties. In order to seek for the most suitable thickness of skin plate, checking panel zone written in some design codes, a calculation formula of skin plate thickness t_s in a weak-axis cover-plate connection is given as follows

$$t_s \geq \frac{(h_b + h_c)}{50}\sqrt{\frac{f_y}{235}} \tag{1}$$

where h_b is the height of H-shaped beam; h_c is the height of I-section column; f_y is the normal yield strength of steel material used in the connection.

5.1 Formula validation in exterior frame joints

According to Eq. (1), the minimum skin plate thickness of specimen SJ-2 should be 13 mm, thus, EST series joints were created with the skin plate thickness of 10, 12, 14 and 16 mm, and the details of EST series joints are shown in Table 2. The failure modes and stress distributions of the skin plate are displayed in Figs. 22 and 23 respectively. The numerical analysis results are listed in Table 3.

It can be observed from Fig. 22 that the overall failure modes of the EST series joints are nearly consistent, and the plastic hinge formed in beam flanges and web beyond the cover-plate range. Fig. 23 also shows that the stress in the skin plate decreased with the increasing of the skin plate thickness.

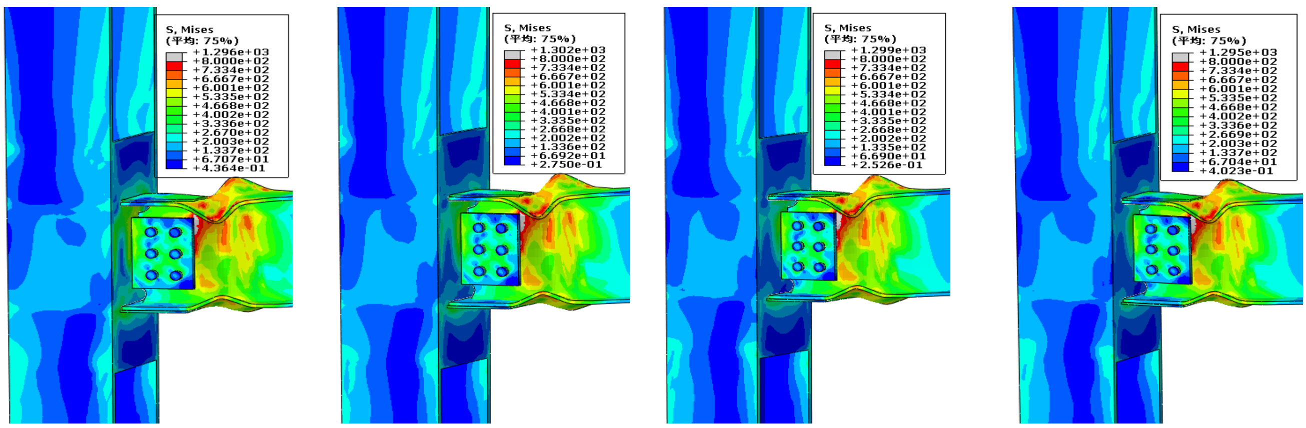

(a) EST-1 (b) EST-2 (c) EST-3 (d) EST-4

Fig. 22 Failure modes of EST series joints

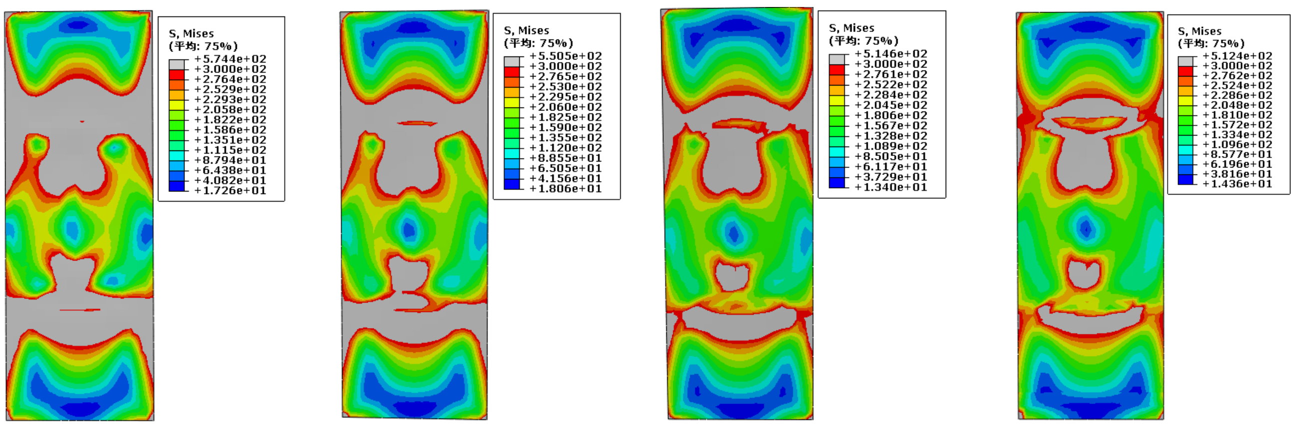

(a) EST-1 (b) EST-2 (c) EST-3 (d) EST-4

Fig. 23 Stress profiles of skin plates of EST series joints

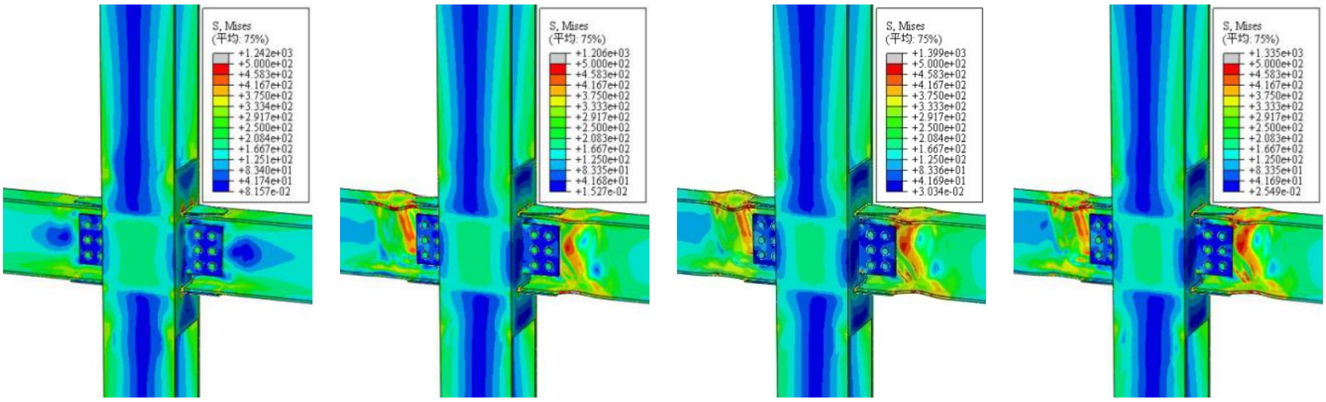

(a) IST-1 (b) IST-2 (c) IST-3 (d) IST-4

Fig. 24 Failure modes of IST series joints

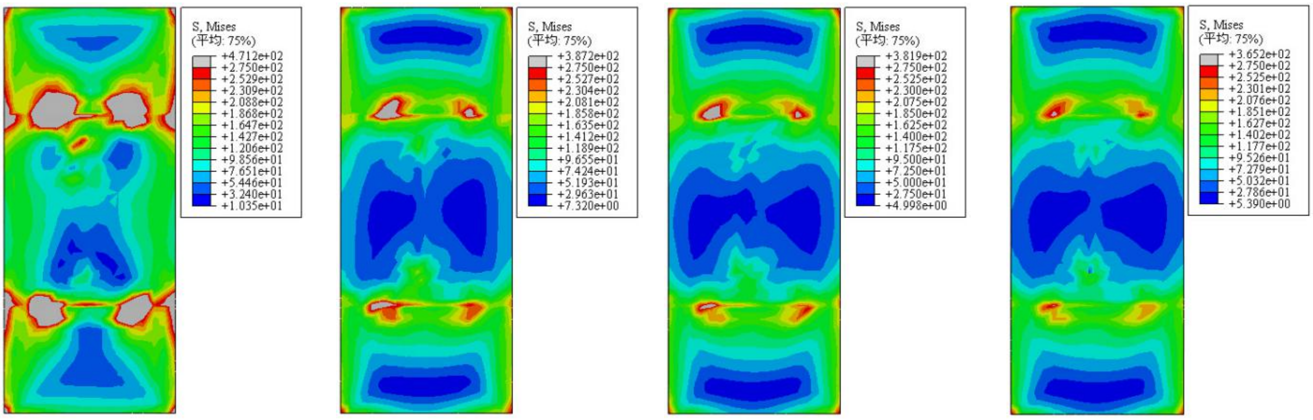

(a) IST-1 (b) IST-2 (c) IST-3 (d) IST-4

Fig. 25 Stress profiles of skin plates of EST series joints

From the calculation data listed in Table 3, the thickness change of skin plate slightly affected the bearing capacity but significantly affected the stiffness, ductility coefficient, and maximum plastic rotation angle. The initial rotation stiffness of EST-4 was 9.5% greater than that of EST-1, and the ductility coefficient of EST-4 was 18.8% higher than that of EST-1, and the maximum plastic rotation angle of EST-1 was 11.4% lower than that of EST-4. The maximum plastic rotation of joints EST-1 and EST-2 did not satisfy the requirement of FEMA267 (1995), due to their thicknesses of the skin plate were lower than 13 mm, calculated by Eq. (1). Thus, it can be concluded that the Eq. (1) is suitable to calculate skin plate thickness of an exterior frame joint.

5.2 Formula validation in interior frame joints

According to Eq. (1), the minimum skin plate thickness of specimen SJ-3 should be 14 mm, thus, IST series joints were created with the skin plate thickness of 12, 14, 16 and 18 mm, and the details of IST series joints are shown in Table 2. The numerical analysis results of IST series joints are listed in Table 4. The failure modes and stress profiles of the skin plate of IST series joints are displayed in Figs. 24 and 25 respectively.

It can be seen form Fig. 24 that the beam plastic hinge of IST-1, whose skin plate thickness was not satisfied Eq. (1), did not form and a high-stress zone existed in the beam flange groove weld, indicating that the too thin skin plate did not provide enough stiffness to force the plastic hinge to form in the beam section. With the increase of the skin plate thickness, the plastic hinge gradually formed in the beam section outward the cover-plate region, indicating that enhancing the thickness of the skin plate is beneficial for beam plastic hinge occurring. Fig. 25 shows that the skin plate stress distributions of IST series joints were consistent with that of EST series joints.

As there was no decline in the load-deflection hysteretic curve of IST-1 numerical analysis, only the calculation results of other three joints in IST series joints are listed in Table 4. The calculation results declared that changing the thickness of the skin plate gently influenced the bearing capacity and joint ductility.

It can be concluded that the Eq. (1) is also suitable to calculate the minimum skin plate thickness of an interior frame joint.

5.3 Formula validation with different steel grade

In order to gain further insight into the applicability of Eq. (1), different steel material grade was adopted in ESM series joints, and grade Q345 steel was considered in this series joints. The true material properties of grade Q345 steel were obtained from the coupon test, with the yield strength of 333.33 MPa, tensile strength of 458.33 MPa, Elastic modulus of 2.06×10^5 MPa, and Elongation of 21.9%. Three exterior frame joints were created and analyzed under beam end cyclic loading in order to investigate the applicability of Eq. (1) for different steel grade steel. According to Eq. (1), the minimum thickness of ESM series joints is 15 mm, thus, ESM series joints were created with the skin plate thickness of 12, 14, 16 mm, and the specimen details are shown in Table 2. The failure modes of ESM series joints are displayed in Fig. 26, and the numerical analysis results are listed in Table 3.

It can be observed from Fig. 26 that the overall failure modes of the ESM series joints are nearly consistent, and the plastic hinge formed fully in beam flanges and web beyond the cover-plate range. From the calculation results listed in Table 3, it can be seen that the thickness change of skin plate strongly impacted the stiffness, ductility coefficient, and maximum plastic rotation angle. The initial rotation stiffness of ESM-3 was 9.5% greater than that of ESM-1, and the ductility coefficient of ESM-3 was 18.8% higher than that of ESM-1, as the maximum plastic rotation angle of ESM-1 was 11.4% lower than that of ESM-3. The maximum plastic rotation of joints EST-1and EST-2 did not satisfy the requirement of FEMA267 (1995) as their thicknesses of skin plate were lower than 15 mm, which was calculated by Eq. (1). Thus, the Eq. (1) is suitable to calculate skin plate thickness for different grade steel with normal yield strength between 235 and 345 MPa.

6. Recommended design procedure

Based on the tests, as well as the parametric-analytic studies and practical specimens design experience, the following design procedure was developed for weak-axis cover-plate moment connection, when column and beam sections had been determined. In 2016, according to the following design procedure, the research team introduced the novel weak-axis cover-plate moment connection proposed in the paper to a real standard industrial park project (Fig. 27), which located Zha Shui County, Shannxi Province, China. Thus, introduced the novel weak-axis cover-plate moment connection has been used in some multi-story steel frames and the total building area is more than 37 thousand square meter. Because there are not any

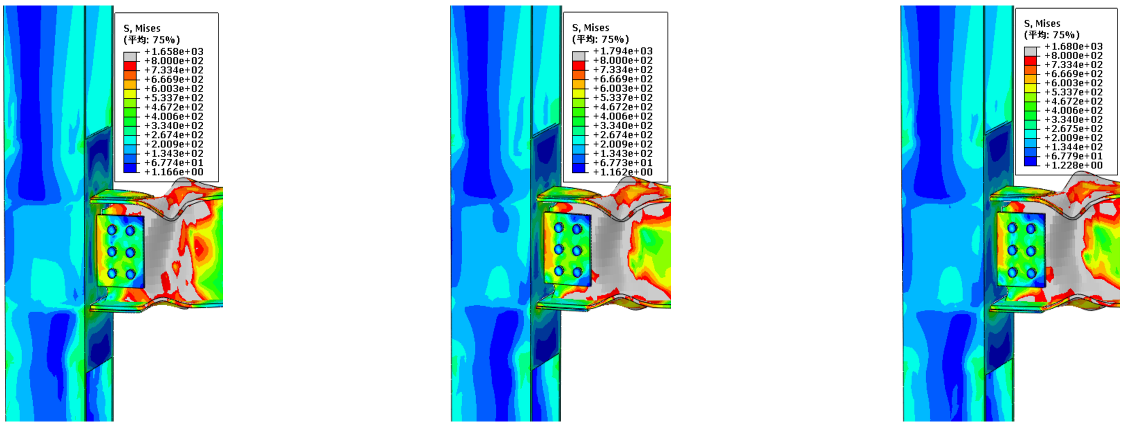

(a) ESM-1 (b) ESM-2 (c) ESM-3

Fig. 26 Failure modes of ESM series joints

(a) Photo of part frames (b) Photo of a steel frame (c) Photo of real connections

Fig. 27 Weak-axis cover-plate moment connections in a real project design references and rules in current design codes about the novel weak-axis cover-plate moment connection in China, the applicability and correctness of recommended design procedure proposed in the paper underwent a rigorous government technical review and have passed the technical review at last.

Step 1: Design of Skin Plate

The geometrical size of skin plate is determined by column section and beam section. Skin plate width equals to the column section height minus the sum of the two column flange thickness, and skin plate minimum height equals to the beam section height plus 300 mm, and skin plate thickness can be calculated by Eq. (1).

Step 2: Design of Cover-Plate

According to to the tests and numerical analysis, the length of cover-plate is better to equal to the 0.5-time height of H-shape beam section. The width of top cover-plate equal to the width of beam flange minus 20mm and the width of bottom cover-plate equals to the width of beam flange plus 20 mm. The thickness of cover-plate is determined by Eq. (2) given as follows.

$$t_{cp} = \min\left(t_{bf}, t_{cf} - t_{bf}\right) \quad (2)$$

where t_{cp} is the thickness of cover-plate; t_{bf} is the thickness of beam flange; t_{cf} is the thickness of column flange.

Step 3: Design of Fillet Weld of Cover-plate and Beam Flange

The bearing capacity must be greater than the design bearing capacity of cover-plate to protect the cover-plate so as to corporate cooperative work with beam flange. Thus, the fillet weld must satisfy the following Eq. (3).

$$0.7h_f(\beta_f \sum l_{w1} + \sum l_{w2}) f_f^w \ge t_{cp} b_{cp} f \quad (3)$$

where, h_f is the height of fillet weld; l_{w1} is the calculation length of a front fillet weld; l_{w2} is the calculation length of a side fillet weld; β_f is an amplifying coefficient and equals to 1.22; f_f^w is the design stress of fillet weld; t_{cp} is the thickness of cover-plate, calculated by Eq. (2); b_{cp} is the width of cover-plate; f is the design strength of cover-plate steel material.

Step 4: Strong Column-Weak Beam Criterion

According to Chinese Code GB50011 (2010), strong column-weak beam criterion is displayed by Eq. (4) shown as follows.

$$\sum W_{pc}\left(f_{yc} - N/A_c\right) \ge \eta \sum W_{pb} f_{yb} \quad (4)$$

where, W_{pc} is plastic section modulus for column; W_{pb} is plastic section modulus for beam; f_{yc} is the yield stress of column material; f_{yb} is the yield stress of beam material; $N$is the axial force on column in compression considering earthquake action; A_c is the gross area of column section; η is a coefficient given in GB50011 (2010).

Step 5: Panel Zone Check

Calculate the volume of panel zone based on box-section of a joint is shown in Eq.(5), and make sure that the yield bearing capacity and design bearing capacity of panel zone satisfy Eq.(6) and Eq.(7). Since the panel zone is composed of two flanges, the panel zone strength requirement is usually easily satisfied.

$$V_{\mathrm{p}} = 1.8 h_{\mathrm{b1}} h_{\mathrm{c1}} t_{\mathrm{w}} \quad (5)$$

$$\psi\left(M_{\mathrm{pb1}} + M_{\mathrm{pb2}}\right)/V_{\mathrm{p}} \le (4/3) f_{y\mathrm{v}} \quad (6)$$

$$\left(M_{\mathrm{b1}} + M_{\mathrm{b2}}\right)/V_{\mathrm{p}} \le (4/3) f_{\mathrm{v}} / \gamma_{\mathrm{RE}} \quad (7)$$

where, V_{p} is the volume of panel zone; h_{b1} is the distance between the center of top and bottom beam flange; h_{c1} is the distance between the centers of column flange; t_{w} is thickness of column flange; M_{pb1} and M_{pb2} are the full plastic bending bearing capacity of both sides beam respectively; Ψ is a factor given in GB50011 (2010); $f_{y\mathrm{v}}$ is the yield shear strength of steel; M_{b1} and M_{b2} are the design moment of both sides beam respectively; $f_{y\mathrm{v}}$ is the design shear strength of steel; γ_{RE} is a coefficient considering earthquake action and equals to 0.75.

Step 6: Design Groove Weld

In China, the groove weld of beam flange often does not require to be calculated, when the quality grade of groove weld is one or two. But it is necessary to take some technical methods to ensure the construction quality of the beam flange groove weld. Use a backing plate and remove it after groove weld is in place and weld metal deposition become cool, and then the edges of the groove weld should be ground smooth to avoid notches.

Step 7: Design of Beam Web Connection

On the assumption of full design moment undertaken by beam flange groove weld, the beam web connection will bear full design shear force. Thus, the design process includes fillet weld design between the shear plate and skin plate and high-strength bolt shear design. Those common design processes are not mentioned here.

7. Conclusions

This paper systematically investigated the mechanical performance of the weak-axis cover-plate connection using the test method and a nonlinear finite element analysis program ABAQUS, based on the experimental studies and numerical analysis results, the following conclusions can be drawn.

- The strains at both edges of the beam flange are greater than the middle's no matter in beam end monotonic loading or column top cyclic loading tests, indicating it is necessary to take same technical methods to ensure the construction quality of the beam flange groove weld, such as using a backing plate and removing it after weld metal deposition become cool.

- Under beam end monotonic loading, the panel zone and welds kept in good condition, and beam flanges and web experienced substantial local buckling deformations outside the cover-plate region. The plastic rotation of the exterior joint can satisfy the requirement of FEMA-267 (1995) of 0.03 rad. While under the column top cyclic loading, only one side connection of interior joint satisfied ANSI/AISC 341-10 that the beam-to-column connections shall be capable of accommodating a story drift angle of at least 0.04 rad while the measured flexural resistance of the connection at the face of the column should equal at least 0.80 M_p of the beam, mainly because the premature fracture of weld between diaphragm and skin plate caused the early crack in beam flange groove weld, then prevented the occurrence of the beam plastic hinge, and also resulting in a drastic drop of the resistance.
- The initial stiffness of FEM and test determined by the inclination of the skeleton curve in the elastic stage matched well, and the inelastic response of the connection in FEM shows the same trend as test results. Then a systemic parametric study was carried out to investigate the structural behavior with variations in: shape of the top cover-plate, length of the cover-plate, thickness of the cover-plate and the skin plate, and also the steel material grade. Changing the shape or the thickness or the length of the cover-plate did not significantly affect the mechanical behaviors of frame joints no matter in exterior joints or interior joints. The length and thickness of the cover-plate recommended by FEMA 267 (1995) is also suitable to the weak-axis cover-plate joint.
- Eq. (1) is suitable to calculate the minimum skin plate thickness for the proposed weak-axis cover-plate connections for different grade steel with normal yield strength between 235 and 345 MPa. And a design procedure is recommended for the weak-axis cover-plate connections.

Acknowledgments

The authors would like to thank the Nature Science Foundation of China (NSFC) (51278061) and the Fundamental Research Funds for the Central Universities-Cultivation of Excellent Doctoral Dissertation of Chang’an University (310828175002) for the financial support.

References

ANSI/AISC 341-10 (2010), Seismic Provisions for structural steel buildings. AISC; Chicago, IL, USA.

Ataollahi, S., Banan, M.R. and Banan, M.R. (2016), “Numerical cyclic behavior of T-RBS: A new steel moment connection”, *Steel Compos. Struct.*, *Int. J.*, **21**(6), 1251-1274.

Driscoll, G.C. and Beedle, L.S. (1982), “Suggestions for avoiding beam-to-column web connection failure”, *Eng. J.*, **19**(1), 16-19.

Engelhardt, M.D. and Sabol, T.A. (1998), “Reinforcing of steel moment connections with cover plates: benefits and limitations”, *Eng. Struct.*, **20**(4-6), 510-520.

FEMA-267 (1995), Interim Guidelines: Evaluation, Repair, Modification and Design of Steel Moment Frames, Report No. SAC-95-02; Washington, D.C., USA.

FEMA-355D (2000), State of the Art Report on Connection Performance; prepared by the SAC Joint Venture for the Federal Emergency Management Agency, Washington, WA, USA.

GB 50011-2010(2010), Code for Seismic Design of Buildings, China Architecture & Building Press; Beijing, P.R. China.

JGJ/T 101 (2015), Specification for seismic test of buildings; China Architecture & Building Press; Beijing, P.R. China.

Kim, T., Whittaker, A.S., Gilani, A.S.J., Bertero, V.V. and Takhirov, S.M. (2002), “Cover-plate and flange-plate steel moment-resisting connections”, *J. Struct. Eng.*, **128**, 474-482.

Lu, L.F., Xu, Y., Zhou, T. and Zheng, H. (2016), “Experimental research on box strengthened joint connection for weak axis of I-section column-H-shaped beam under monotonic loading”, *J. Build. Struct.*, **37**(2), 73-80.

Lu, L., Xu, Y. and Zheng, H. (2017), “Investigation of composite action on seismic performance of weak-axis column bending connections”, *J. Constr. Steel Res.*, **129**, 286-300.

Nassani, D.E., Chikho, A.H. and Akgonen, A.I. (2017), “Semi-rigidity of cap plate and extended end plate connections”, *Steel Compos. Struct.*, *Int. J.*, **23**(5), 493-499.

Rezaifar, O. and Younesi, A. (2016), “Finite element study the seismic behavior of connection to replace the continuity plates in (NFT/CFT) steel columns”, *Steel Compos. Struct.*, *Int. J.*, **21**(1), 73-91.

Shim, H.J., Lee, E.T., Kim, S.B. and Kim, S.S. (2014), “Development and performance evaluation of weak-axis column bending connections for advanced constructability”, *Int. J. Steel Struct.res*, **14**(2), 369-380.

Xu, Y.L., Lu, L.F., and Zhang, B.C. (2016), “Influence factor analysis on hysteretic behavior of weak-axis cover-plate connections of I-section column in frame side joint”, *J. Southeast Univ.* (*Natural Science Ed.*), **46**(3) 537-544.

Zahrai, S.M., Mirghaderi, S.R. and Saleh, A. (2017a), “Increasing plastic hinge length using two pipes in a proposed web reduced beam section, an experimental and numerical study”, *Steel Compos. Struct.*, *Int. J.*, **23**(4), 421-433.

Zahrai, S.M., Mirghaderi, S.R. and Saleh, A. (2017b), “Tubular Web Reduced Beam Section (TW-RBS) connection, a numerical and experimental study and result comparison”, *Steel Compos. Struct.*, *Int. J.*, **23**(5), 571-583.

CC